Int. J. Electrochem. Sci., 12 **(2017)** 3221 – 3230, doi: 10.20964/2017.04.43

International Journal of
ELECTROCHEMICAL
SCIENCE
www.electrochemsci.org

Magnetic Activation of a $LiFePO_4$@C Composite Cathode Material

Chun-ping Hou[1,2], *Yong Ma*[1], *Hao Zhang*[1], *Wang-chang Geng*[1], *and Qiu-yu Zhang*[1,*]

[1] School of Science, Northwestern Polytechnical University, Xi'an Shaanxi, 710129, P.R. China
[2] Ningxia BOLT Technologies Co., Ltd., Yinchuan Ningxia, 750011, P.R. China
[*]E-mail: qyzhang@nwpu.edu.cn

Received: 31 December 2016 / *Accepted:* 15 February 2017 / *Published:* 12 March 2017

A $LiFePO_4$@C composite cathode material was prepared from LiH_2PO_4, $FeC_2O_4 \cdot 2H_2O$ and glucose via a ball-milling and spray-drying technique and was then processed by carbothermal reduction and a magnetizing treatment. The samples were characterized by VSM, XRD, SEM, EDS, XPS and electrochemical analyses. The results reveal that LFP@C has a spherical morphology with a microstructure of aggregated nanoparticles. The magnetizing treatment can change the magnetic properties of the as-prepared sample slightly and therefore slightly enhance the initial discharge capacity. The sample subjected to a 72 h-magnetizing treatment delivers an initial discharge capacity of 155 mAh g^{-1} at 0.1 C, an initial coulomb efficiency of 96.03 %, as well as improved low-temperature discharge characteristics. The CV curves and EIS demonstrated that the magnetizing treatment can reduce the polarization and charge-transfer resistance for LFP@C composite electrodes. The magnetizing treatment, which plays a role in the magnetic activation of the sample, results in the improvement of the electrochemical properties to acertain extent for LFP@C composite electrodes. In addition, there is no effect on the crystal structure or morphology, but the peak of the binding energy for Fe 2p1/2 changes.

Keywords: Cathode material; $LiFePO_4$; Magnetic activation; Li-ion batteries

1. INTRODUCTION

Lithium ion batteries (LIBs) have many demonstrated advantages such as high working potential, low self-discharge rate, excellent energy density and outstanding long cycle life [1-3]. Recently, considerable efforts have been devoted to expanding their practical applications in high power situations, such as electric vehicles (EVs) and hybrid electric vehicles (HEVs), which require LIBs to exhibit excellent calendar-life [4, 5]. $LiFePO_4$ has already been considered as an important

battery cathode material in EVs. The specific characteristics of $LiFePO_4$, such as cycle stability, safety, environmental friendliness, flat voltage profile and potential low cost, make this material the most promising electrode material for use in LIBs for EVs applications [6, 7].

However, there are still a number of technical challenges to be overcome in its wide-spread applications. The drawbacks of $LiFePO_4$ include its relatively low theoretical capacity (170 mAh g^{-1}), low tap density, poor electronic conductivity and low ionic diffusivity [8, 9]. Tremendous efforts have been made towards developing this material, such as preparing nano-scale particles [10-12], doping [13, 14], coating with carbon [15, 16], loading with conductive additives [17-19] or developing new synthesis techniques [20-23] to improve its rate capability, discharge capacity, low-temperature performance, etc.

Generally, the magnetism of a transition-metal material or a magnetic field will influence the properties or structures of a material [24-29]. However, there are scarcely any reports about the effect of the magnetizing treatment on the $LiFePO_4$ cathode material, especially for LIBs. In 2014, Qiao et al firstly prepared the $LiFePO_4$/C composite with excellent rate capability and cycle performance by hydrothermal synthesis along with a magnetic treatment method due to the removal of Fe^{3+} cations [30]. In this work, this novel magnetizing treatment technique was developed to improve the electrochemical performance of the $LiFePO_4$@C composite cathode material (LFP@C).

2. EXPERIMENTAL

2.1. Preparation and characterizations

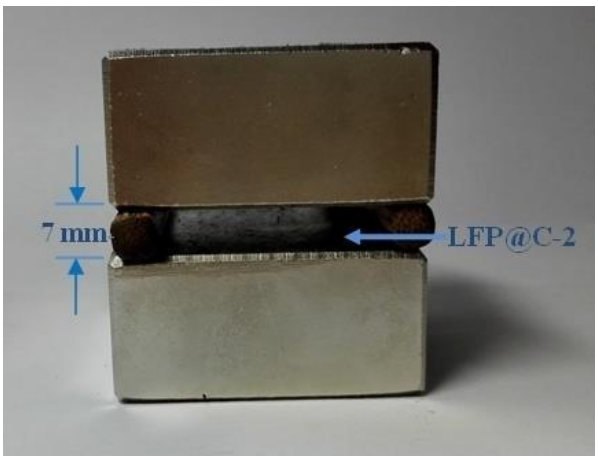

Figure 1. Digital photo of the magnetization of LFP@C-2.

The $LiFePO_4$@C composite cathode material was prepared from lithium dihydrogen phosphate, LiH_2PO_4 (≥99.9 %, Sichuan State Lithium Materials Co., Ltd.), iron (II) oxalate dihydrate, $FeC_2O_4 \cdot 2H_2O$ (≥99.5 %, Hefei Asialon Chemical Co., Ltd.) and glucose (AR, Sinopharm Chemical Reagent Co., Ltd) via a ball-milling and spray-drying technique, then processed with carbothermal reduction (CTR) at 700 °C for 10 h under a pure N_2 atmosphere, and finally magnetized between two square magnets (L*W*H=50 mm*50 mm*25 mm, 8000 Gs, Shanghai) for different lengths of time.

LFP@C-1 was not magnetized at all and was used for comparison, while LFP@C-2 was magnetized in the magnetic field of 8000 Gs for 72 h, as shown in Fig. 1.

The phase identification of powder samples was conducted with a XRD-7000S diffractometer (Shimadza, Japan) using Cu Ka radiation (λ=0.15423 nm). The surface morphologies of the samples were observed with a scanning electron microscope (JEOL JSM-6700F, Japan), and the phase compositions were investigated with an Inca X-act EDS analyser (Oxford Instruments, UK). X-ray photoelectron spectra (XPS) were obtained by using a Kratos Axis Ultra DDL spectrometer (Shimadza, Japan). The magnetic properties of the samples were measured at room temperature using a Quantum Design VersaLab vibrating sample magnetometer (VSM).

2.2 Electrochemical studies

The electrochemical properties of samples were studied via assembling CR2025 coin cells. The composite electrodes were prepared by mixing the as-synthesized LFP@C composite with carbon black and polyvinylidene fluoride (PVDF) in a weight ratio of 80:13:7 in N-methylpyrrolidone (NMP) to form a homogeneous slurry. Then, the mixtures were coated on an aluminium foil and punched to disks. After drying under ambient condition, the disks were further dried in a vacuum oven at 120 °C for 12 h. Finally, the cells were assembled in an Ar-filled glove box (LABSTAR 1250/750, MBRAUN) using lithium foil as the counter and reference electrode, a polypropylene micro-porous film (Cellgard2400) as the separator, 1 M $LiPF_6$ in ethylene carbonate (EC), dimethyl carbonate (DMC) and diethyl carbonate (DEC) (1:1:1, v/v/v) (Guangzhou Tinci) as the electrolyte. The LAND battery testing system (LAND CT2001A, Wuhan, China) was used to perform the galvanostatic charge/discharge tests in the potential range of 2.5-4.1 V. Both electrochemical impedance spectroscopy (EIS) and cyclic voltammetry (CV) measurements were performed on an Electrochemical Workstation (CHI660E, Shanghai, China) at room temperature. The spectra were potentiostatically measured by applying an ac voltage of 5 mV over the frequency range from 10^5 Hz to 10^{-2} Hz. The CV measurements were carried out in the range of 2.3-4.3 V with a 0.1 mV s^{-1} scan rate.

3. RESULTS AND DISCUSSION

Fig. 2 (a) shows the XRD patterns of LFP@C-1 and LFP@C-2. Although their preliminary treatments are different, both samples present very similar XRD diffraction peaks corresponding to orthorhombic $LiFePO_4$ (JCPDS No. 40-1499). No impurity peaks are observed in the X-ray patterns [31], demonstrating that the magnetizing treatment has not changed the crystal structure of LFP@C-2.

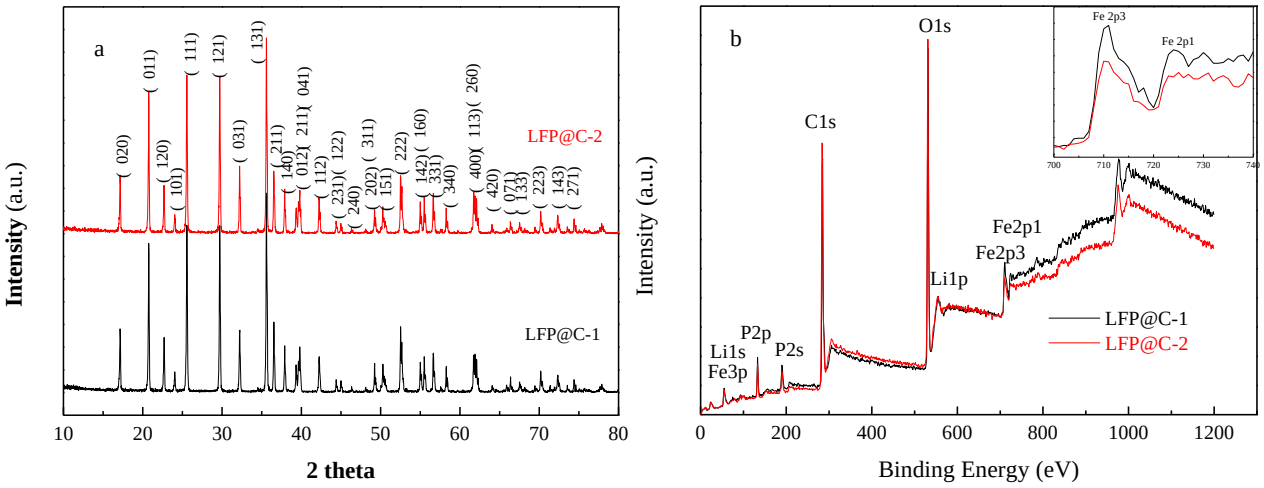

Figure 2. (a) XRD patterns and (b) XPS spectra for LFP@C-1 and LFP@C-2.

Fig. 2 (b) shows that XPS is been well-suited for the evaluation of the valence and electronic states of the olivine $LiFePO_4$ cathode materials. The main binding energies (BEs) of the Li 1s, Fe 2p, P 2p, O 1s and C 1s peaks are determined to be 55 eV, 710 eV, 133 eV, 531 eV, and 284 eV, respectively. This is in good agreement with the previous report that the Fe 2p peak split into 2p1/2 and 2p3/2 due to the spin-orbit coupling for the LFP@C-1 composite (see Table 1), which are very close to the standard peaks (2p1/2=723.6 eV, 2p3/2=710.4 eV) [32]. Each part consists of a main peak and a corresponding satellite peak at BEs of 710 and 723 eV for Fe 2p3/2 and Fe 2p1/2, respectively. In fact, the appearance of satellite peaks or shoulder peaks is a typical characteristic feature of transition metal ions with partially filled d-orbits. Here, the two distinct BE peaks are attributed to the characteristic of the valence of the Fe^{2+} state in the $LiFePO_4$. Compared to unmagnetized LFP@C-1, the enhancement of the BEs of the P 2p and O 1s peaks for LFP@C-2 means the heightening of the P-O bond energy with magnetization. At the same time, the strength of the BE of Fe 2p3/2 decreases and the BEs of the Fe 2p1/2 and Fe 3p peaks, which appear at 723.65 eV and 56.55 eV for LFP@C-1, have not been observed for LFP@C-2 after magnetization. Therefore, the magnetizing treatment has an effect on the valence and electronic states of the olivine $LiFePO_4$ cathode material.

Table 1. Binding energy of Li, P, O, Fe and C for LFP@C-1 and LFP@C-2, respectively.

Sample	Binding energy (eV)						
	Li 1s	P 2p	O 1s	Fe 2p		Fe 3p	C 1s
LFP@C-1	55.35	133.35	531.45	710.31	723.65	56.55	284.65
LFP@C-2	55.35	133.25	531.35	710.45	-	-	284.45

It has not been clearly observed that the morphology of LFP@C-1 is different from that of LFP@C-2 in Fig. 3. The secondary particle of LFP@C is a spherical conglomeration of many nanoparticles. The elementary nanoparticles are approximately 300 nm in diameter. EDS semi-quantitative analysis for area A and area B in Fig. 3 confirm that there are nearly no apparent differences in composition between LFP@C-1 and LFP@C-2 (see Table 2).

Table 2. Phase compositions of Area A and Area B for LFP@C-1 and LFP@C-2 by EDS semi-quantitative analysis, respectively

Area	Composition (mass %)				
	C	O	P	Fe	Total
A	12.35	30.38	20.73	36.55	100
B	12.86	29.73	19.90	37.51	100

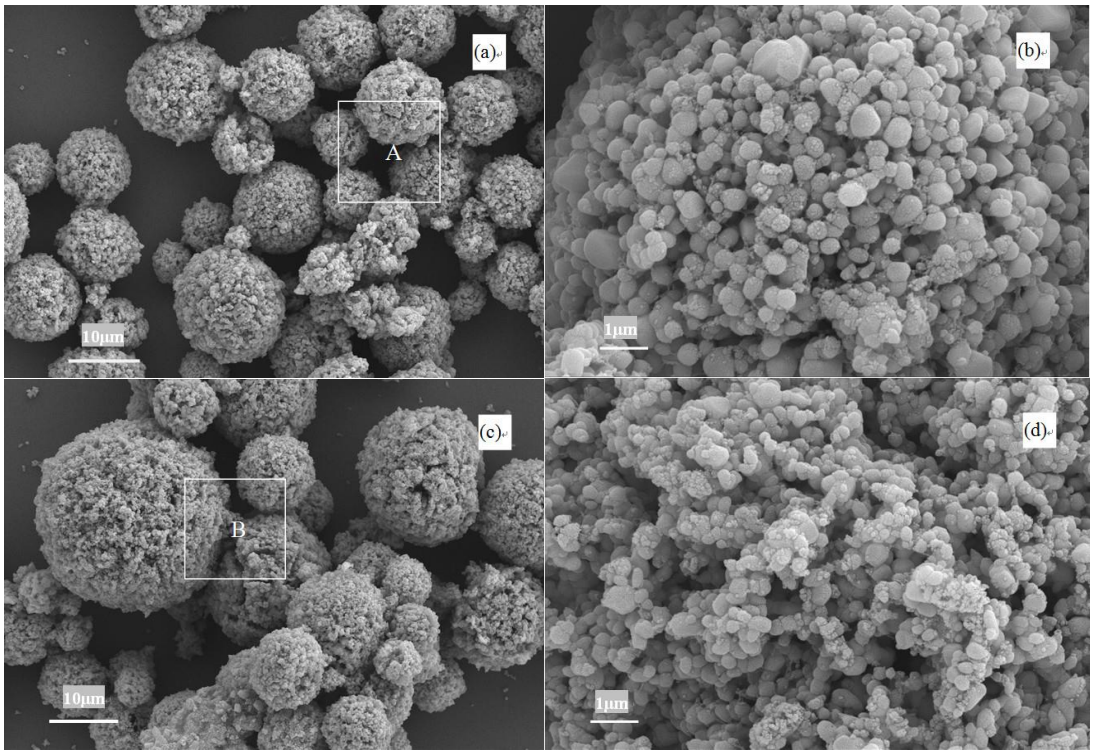

Figure 3. FE-SEM images of LFP@C-1 (a, b) and LFP@C-2 (c, d).

Fig. 4 presents the VSM curves ofLFP@C-1 and LFP@C-2 measured at room temperature. As shown in Fig. 4, the magnetism of LFP@C-2 is slightly higher than that of LFP@C-1, indicating that the magnetic field has an effect upon LFP@C to a certain extent. Fig. 5 (a) illustrates the charge/discharge curves of the first cycle of LFP@C-1 and LFP@C-2 at a rate of 0.1 C at room temperature. In the potential range of 2.5-4.1 V, the discharge capacities for LFP@C-1 and LFP@C-2 are 150.2 and 155 mAh g^{-1}, respectively. Meanwhile, initial coulomb efficiencies of 95.97 % and 96.03 % are obtained, respectively. The LFP@C-2 retains a higher capacity and a superior initial coulomb

efficiency. At room temperature, the differences of the charge and discharge plateau potentials (vs. Li^+/Li) between LFP@C-1 and LFP@C-2 are negligibly small.

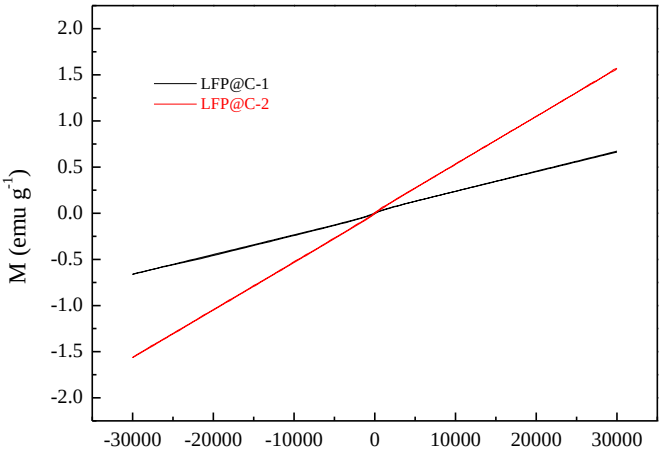

Figure 4. VSM curves of LFP@C-1 and LFP@C-2 measured at room temperature.

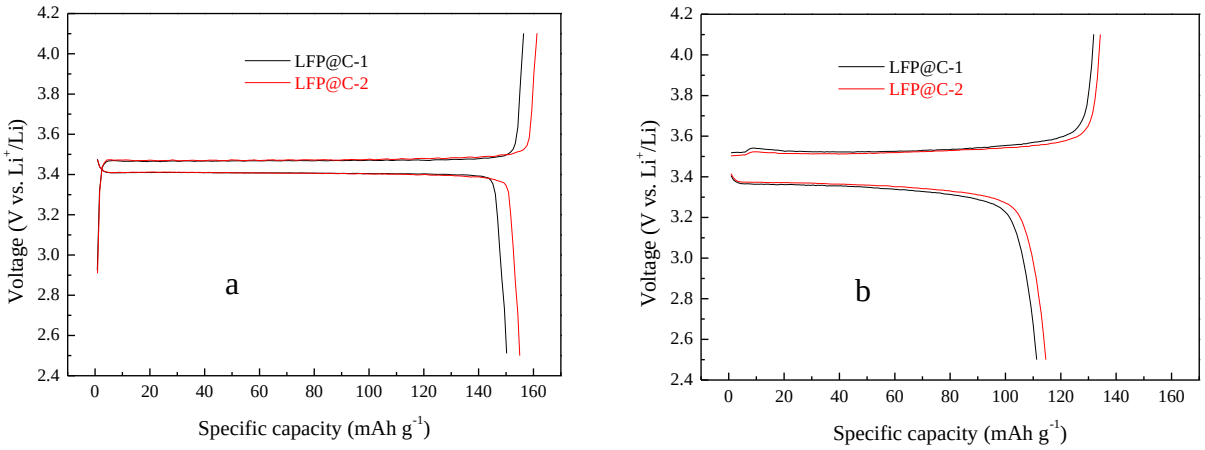

Figure 5. Charge-discharge curves of LFP@C-1 and LFP@C-2 in the potential range of 2.5-4.1 V at a rate of 0.1 C: (a) at room temperature, and (b) at -10 °C.

However, the differences between charge and discharge potential increase with decreasing test temperature, as seen in Fig. 5 (b). At -10 °C, the discharge capacities for LFP@C-1 and LFP@C-2 are 111.3 and 114.6 mAh g^{-1} in the potential range of 2.5-4.1 V, respectively. At the same time, initial coulomb efficiencies of 84.38 % and 85.33 % are obtained, respectively. LFP@C-2 still holds a higher capacity and better initial coulomb efficiency. At -10 °C, the differences of the charge and discharge plateau potentials (vs. Li^+/Li) between LFP@C-1 and LFP@C-2 become more apparent. The potential difference between the charge and discharge plateaus correlates to an important electrochemical phenomenon denoted as electrochemical polarization, which is an important factor in evaluating the electrode reaction kinetics during cycling. Therefore, the larger the potential difference between the charge and the discharge plateaus, the severer the polarization of the electrode, which is caused by the

discharge reaction of $LiFePO_4$ [17]. Less polarization correlates to better reaction kinetics. With decreasing temperature, more serious polarization occurred; therefore, the discharge plateaus reduce and the capacity drops simultaneously. However, compared with LFP@C-1, LFP@C-2 with magnetizing treatment still exhibits a lower polarization and a superior capacity. Thus, it is believed that the appropriate magnetizing treatment can contribute to the faster reaction kinetics of LFP@C-2. The improved electrochemical performances may result from the magnetic activation. Gu et al report that the commonly used transition FM metals are Fe, Co and Ni since the 3d bands of these metals are split by the exchange energy (approximate 1-2 eV), giving two markedly different bands, i.e., spin-up (with a spin parallel to the magnetization) and spin-down (with a spin antiparallel to the magnetization) electrons at the Fermi level. The electrons in a magnetic material can give different resistances and mean free paths due to the difference in density of states at the Fermi level ($N(E_F)$) of these two spins, which leads to different scattering rates when an external magnetic field is applied [29]. In this work, the external magnetic field applied gives a positive effect on the improvement of conductivity of the as-prepared LFP@C-2 composite. The magnetized sample also exhibits a better rate capability and cycle performance, as shown in Fig. 6 (a) and (b). The magnetized LFP@C material delivers a discharge capacity of 159 mAh g^{-1} after two cycles, and which is a higher capacity among the literatures reported (as listed in Table 3).

Table 3. The discharge capacities of the $LiFePO_4$/C with different treatment methods as reported.

Capacity (mAh g^{-1})	Rate (C)	Refences
162	0.1	(10)
145	1/9	(11)
154	0.2	(13)
169	0.1	(15)
158	0.1	(16)
149	0.1	(17)
160	0.1	(18)
150	0.8	(19)
150	0.1	(20)
155	0.1	(21)
168	0.5	(23)
155-159	0.1	This work

The cyclic voltammetric profiles of the first cycles for LFP@C-1 and LFP@C-2 are shown in Fig. 7 (a). The well-defined redox doublet located at 3.73/3.21 V and 3.70/3.22 V represents the inter-transformation of Fe^{2+}/Fe^{3+} during the Li^+ intercalation/de-intercalation process for LFP@C-1 and LFP@C-2, respectively. The symmetrical shapes of the anodic/cathodic peaks indicate that the electrochemical intercalation/de-intercalation of lithium ions in the electrode materials is reversible. It should be noted that the gap between the redox peaks of the LFP@C-2 electrode is narrower and the

peak shape is sharper and higher than that of the LFP@C-1 electrode, suggesting that the former has less polarization and better kinetics for lithium insertion and extraction [33].

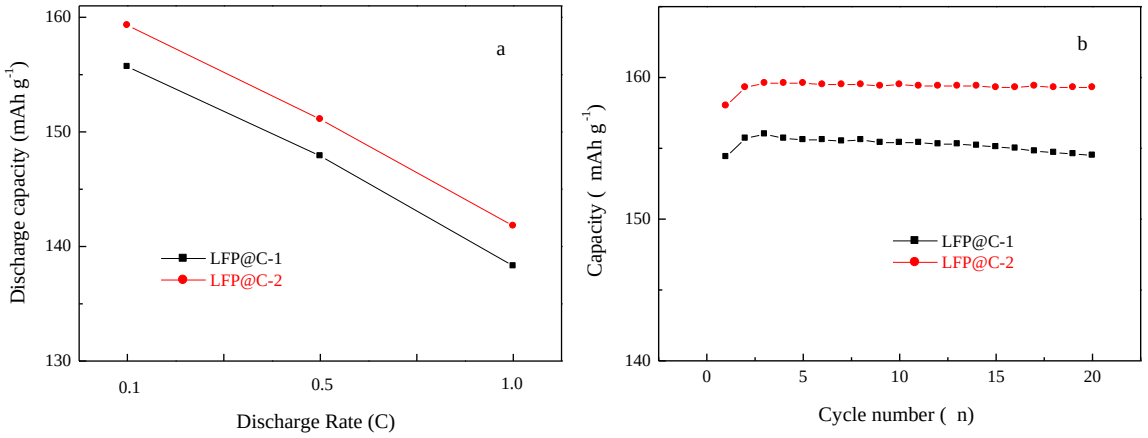

Figure 6. (a) Rate capability and (b) cycle performances for LFP@C-1 and LFP@C-2 electrodes.

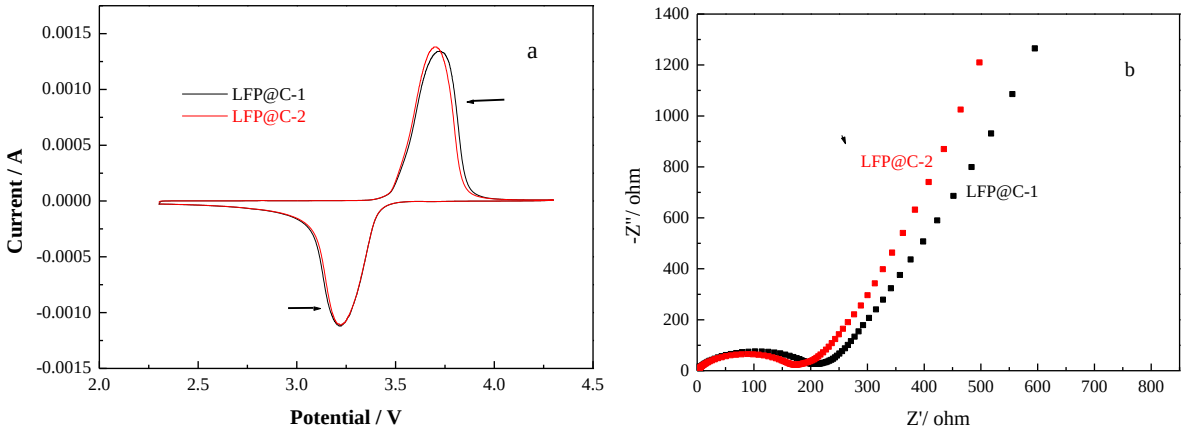

Figure 7. (a) Cyclic voltammograms of the first cycles for LFP@C-1 and LFP@C-2; (b) The Nyquist plots for LFP@C-1 and LFP@C-2 electrodes in the frequency range between 10^5 Hz and10^{-2} Hz.

The Nyquist plots for LFP@C-1 and LFP@C-2 in the frequency range between 10^5 Hz and10^{-2} Hz are shown in Fig. 7 (b). Both electrochemical impedance spectra are combinations of a depressed semicircle at high frequencies and a straight line at low frequencies. The depressed semicircle in the high frequency region is attributed to the charge transfer process. The numerical value of the semicircle diameter on the Z_{re} axis is approximate to the charge-transfer resistance (R_{ct}). In the low frequency region, the straightline represents a typical Warburg behaviour, which corresponds to the diffusion of lithium ions in the active cathode material. The diffusion coefficient of lithium ions could be calculated from the low frequency spots, according to the literatures [34, 35]. The smaller diameter

of the EIS semicircle for the LFP@-2 electrode than that for the LFP@-1 electrode indicates that the magnetizing action decreases the charge-transfer resistance for the LFP@C-2 electrode.

The magnetizing treatment of the LFP@C composite cathode material could enhance its discharge capacity, not only at room temperature but also at low temperature such as -10 °C. The magnetizing treatment of LFP@C is also favourable to reduce electrochemical impedance. We named this helpful magnetizing treatment "magnetic activation". We have inferred that the reason for electrochemical improvement upon magnetizing treatment of the LFP@C may be that the magnetic field brings about the change of spin state of the electrons of the electro-active species, and this contributes to the lower polarization of the electrode and charge-transfer resistance. To confirm the mechanism of the changes, further studies are under way. Magnetizing treatment is very promising and of significance for the industrialization of the LFP@C material as well.

4. CONCLUSIONS

The LFP@C-2 composite cathode material was prepared by a ball-milling and spray-drying technique, and then processed with carbothermal reduction, and finally magnetized between two square magnets for 72 h. The results reveal that the LFP@C composite has a spherical morphology with the microstructure of aggregated nanoparticles. The magnetizing treatment can change the magnetic properties of the as-prepared sample slightly and therefore enhanced the initial discharge capacity of the sample a little. The sample with 72 h-magnetizing delivers an initial discharge capacity of 155 mAh g^{-1} at 0.1 C and an initial coulomb efficiency of 96.03 %, as well as superior low-temperature discharge characteristics. The CV curves and the EIS demonstrate that the magnetizing treatment can reduce the polarization and also decrease the charge-transfer resistance of the LFP@C-2 composite electrode. The magnetization leads to improvement of the electrochemical properties of LFP@C to a certain extent and a change in the peak of binding energy for Fe 2p1/2, but has no effect on its crystal structure and morphology. The application of magnetizing treatment on the LFP@C composite cathode material plays the role of magnetic activation.

ACKNOWLEDGEMENTS
This work was supported by the Science and Technology Innovation Leader Program of Ningxia Hui Autonomous Region, the Key Research Project of Ningxia Hui Autonomous Region (2016), and the Key Research Project of Beifang Univesity of Nationality (grant 2015KJ30).

References

1. J. M. Tarascon and M. Armand, *Nat.*, 414 (2001) 359.
2. J. B. Goodenough and Y. Kim, *Chem. Mater.*, 22 (2010) 587.
3. K. Zaghib, A. Mauger, H. Groult, J. Goodenough and C. Julien, *Mater.*, 6 (2013) 1028.
4. B. Scrosati, M. Bottini and T. Mustelin, *Nat. Nanotech.*, 2 (2007) 598.
5. O. K. Park, Y. Cho, S. Lee, H.-C. Yoo, H.-K. Song and J. Cho, *Energy Environ. Sci.*, 4 (2011) 1621.

6. A. K. Padhi, K. S. Nanjundaswamy and J. B. Goodenough, *J. Electrochem. Soc.*, 144 (1997) 1188.
7. Z. Gong and Y. Yang, *Energy Environ. Sci.*, 4 (2011) 3223.
8. W. J. Zhang, *J. Power Sources*, 196 (2011) 2962.
9. H. Zhang, D. Liu, X. Qian, C. Zhao and Y. Xu, *J. Power Sources*, 249 (2014) 431.
10. G. Wang, H. Liu, J. Liu, S. Qiao, G. M. Lu, P. Munroe and H. Ahn, *Adv. Mater.*, 22 (2010) 4944.
11. X.-L. Wu, L.-Y. Jiang, F.-F. Cao, Y.-G. Guo and L.-J. Wan, *Adv. Mater.*, 21 (2009) 2710.
12. K.-X. Wang, X.-H. Li and J.-S. Chen, *Adv. Mater.*, 27 (2015) 527.
13. W. Wang, Y. Qiao, L. He, L. Kong and M. Zhao, *Ionics*, 21 (2015) 2119.
14. Y. P. Huang, T. Tao, Z. Chen, W. Han, Y. Wu, C. Kuang, S. Zhou and Y. Chen, *J. Mater. Chem. A*, 2 (2014) 18831.
15. C. Zhu, Y. Yu, L. Gu, K. Weichert and J. Maier, *Angew. Chem. Int. Edit.*, 50 (2011) 6278.
16. Y. Wu, Z. Wen and J. Li, *Adv. Mater.*, 23 (2011) 1126.
17. Y. Yin, M. Gao, H. Pan, L. Shen, X. Ye, Y. Liu, P. S. Fedkiw and X. Zhang, *J. Power Sources*, 199 (2012) 256.
18. N. D. Trinh, M. Saulnier, D. Lepage and S. B. Schougaard, *J. Power Sources*, 221 (2013) 284.
19. H. Kim, H. Kim, S. W. Kim, K. Y. Park, J. Kim, S. Jeon and K. Kang, *Carbon*, 50 (2012) 1966.
20. J. Liu, M. N. Banis, Q. Sun, A. Lushington, R. Li, T.-K. Sham and X. Sun, *Adv. Mater*, 26 (2014) 6472.
21. Y. Ren and P. G. Bruce, *Electrochem. Soc.*, 17 (2012) 60.
22. C.-W. Ahn, J.-J. Choi, J. Ryu, B.-D. Hahn, J.-W. Kim, W.-H. Yoon, J.-H. Choi and D.-S. Park, *Carbon*, 82 (2014) 1.
23. X. Guo, Q. Fan, L. Yu, J. Liang, W. Ji, L. Peng, X. Guo, W. Ding and Y. Chen, *J. Mater. Chem. A*, 1 (2013) 11534.
24. R. J. Clément, A. J. Pell, D. S. Middlemiss, F. C. Strobridge, J. K. Miller, M. S. Whittingham, L. Emsley, C. P. Grey and G. Pintacuda, *J. Am. Chem. Soc.*, 134 (2012) 17178.
25. D. Arčon, a. Zorko, P. Cevc, R. Dominko, M. Bele, J. Jamnik, Z. Jagličić and I. Golosovsky, *J. Phys. Chem. Solids*, 65 (2004) 1773.
26. Y. Ma, M. Qiao, C. Hou, Y. Chen, M. Ma, H. Zhang and Q. Zhang, *RSC Adv.*, 5 (2015) 103064.
27. Y. Ma, M. Qiao, Y. Chen, C. Hou, B. Zhang and Q. Zhang, *RSC Adv.*, 5 (2015) 9986.
28. M. M. Rahman, J.-Z. Wang, R. Zeng, D. Wexler and H. K. Liu, *J. Power Sources*, 206 (2012) 259.
29. H. Gu, X. Zhang, H. Wei, Y. Huang, S. Wei and Z. Guo, *Chem. Soc. Rev.*, 42 (2013) 5907.
30. Y. Qiao, L. Pan, P. Jia, H. Wang, L. Kong, W. Gao and X. Wang, *Mater. Lett.*, 137 (2014) 432.
31. L. Pang, M. Zhao, X. Zhao and Y. Chai, *J. Power Sources*, 201 (2012) 253.
32. A. Naik, J. Zhou, C. Gao and L. Wang, *Electron. Acta*, 142 (2014) 215.
33. X. Sun, J. Li, C. Shi, Z. Wang, E. Liu, C. He, X. Du and N. Zhao, *J. Power Sources*, 220 (2012) 264.
34. H. Liu, C. Miao, Y. Meng, Y.-B. He, Q. Xu, X. Zhang and Z. Tang, *Electron. Acta*, 130 (2014) 322.
35. S. Tao, W.-f. Huang, G.-x. Wu, X.-b. Zhu, X.-b. Wang, M. Zhang, S.-h. Wang, W.-s. Chu, L. Song and Z.-y. Wu, *Electron. Acta*, 144 (2014) 406.